Available online at www.sciencedirect.com
SCIENCE DIRECT®
International Journal of Heat and Fluid Flow 24 (2003) 77–90
International Journal of HEAT AND FLUID FLOW
www.elsevier.com/locate/ijhff

Forcing of unsteady separated flow and convective heat transfer via bulk upstream oscillations

A. Bouhadji, N. Djilali *

Department of Mechanical Engineering, University of Victoria, Victoria, B.C., Canada V8W 3P6

Received 31 January 2002; accepted 16 July 2002

Abstract

Simulations are presented for the unsteady separated-reattaching flow and associated heat transfer over a long rectangular plate subjected to an oscillatory inlet velocity, $U = 1 + A_p \sin 2\pi f_p t$. The two-dimensional simulations are performed at a Reynolds number of 1000 by solving the time-dependent Navier–Stokes and energy equation using a finite volume method. The computations are performed on a 300×100 grid, using centered second-order accurate spatial discretization, and a third-order time-stepping scheme. The effect of forcing is investigated by exploring the response of the flow over a range of frequencies up to the 60th harmonic of the natural vortex shedding frequencies and for velocity perturbation amplitudes up to 20% of the free stream. Forcing of the flow is found to radically alter the dynamics of the flow and results in significantly higher local heat transfer rates.

Keywords: Unsteady flow; Flow control; Forcing; Bluff body flow; Flow separation; Numerical simulation; Vortex dynamics; Heat transfer enhancement

1. Introduction

Upstream perturbations or acoustic forcing are inherent to the operation of many fluid dynamic systems and devices. In bluff body flows, such forcing can radically alter the structure of the separated flow and is viewed as a possible means of achieving flow control in order to, for example, reduce separation or drag, or enhance mixing and heat/mass transfer. The proper design and/or control of systems with separated flows and upstream perturbations requires a better understanding of the dynamics of the large (coherent) structures, and of the effect of parameters such as forcing frequency and amplitude. To address some of these issues, a numerical investigation of the flow over a bluff rectangular plate subjected to oscillatory upstream perturbations was undertaken.

The effect of pulsatile inlet conditions on separated flows has been of particular interest in biomedical flows. Tutty and Pedley (1993) have simulated oscillatory flow in a step channel and Rosenfeld (1995) investigated pulsatile separated flow in a constricted flow channel. The key parameter characterizing such flows is the non-dimensional pulsating frequency, or Strouhal number, f_p. An interesting feature reported by Rosenfeld is the asymptotic approach towards the unperturbed solution as f_p becomes large. Orellano and Wengle (2000) have shown in their large-eddy simulation of flow over a fence that local forcing results in a reduction of the mean reattachment length, again with the higher reductions (up to 36%) occurring for low frequency forcing.

In the present paper we present numerical simulations for the flow and convective heat transfer over a blunt flat plate at $Re = 1000$. The flow over a bluff flat plate is a particularly attractive benchmark configuration that simplifies the study of separated-reattaching flows, particularly from a numerical standpoint. This flow configuration, shown in Fig. 1, has the advantage of well defined parameters: the location of separation is fixed; the shear layer at separation is thin; and the upstream boundary conditions are simple and unambiguous. For sufficiently large Reynolds numbers, the separating shear layer becomes unstable, and transition to turbulence occurs soon after separation. Further

* Corresponding author. Tel.: +1-250-7216034; fax: +1-250-7216051.
E-mail address: ndjilali@uvic.ca (N. Djilali).

0142-727X/02/$ - see front matter © 2002 Elsevier Science Inc. All rights reserved.
PII: S0142-727X(02)00201-1

Nomenclature

B_r	blockage ratio, $B_r = d/H$
d	thickness of the plate
H	height of the computational domain
L_d	distance to the outlet boundary from the separation point
L_u	distance to the inlet boundary from the separation point
L_z	spanwise dimension
f_n	non-dimensional natural vortex shedding frequency, $f_n = f_n^* d/U_0$
f_p	non-dimensional pulsating frequency, $f_p = f_p^* d/U_0$
A_p	Velocity perturbation amplitudes
Re	Reynolds number based on thickness of the plate, $Re = U_0 d/\nu$
U_i	non-dimensional velocity components, $U_i = U_i^*/U_0$
U_0	free stream velocity
x_i	non-dimensional cartesian coordinate based on thickness of the plate $(x^*/d, y^*/d)$
$\bar{x}_r$	non-dimensional mean reattachment length (time-averaged); $\bar{x}_r^*/d$
$\bar{x}_{rn}$	non-dimensional natural mean reattachment length (no perturbation); $\bar{x}_{rn}^*/d$
$\overline{X}_r$	Normalized mean reattachment length, $\overline{X}_r = \bar{x}_r/\bar{x}_{rn}$
T	non-dimensional temperature; $T = T^*/T_0$, where T_0 is a reference temperature
$\overline{Nu}_x$	mean Nusselt number (time-averaged)
I_N	Spatial averaged Nusselt number, $I_N = \frac{1}{L_d}\int_0^{L_d} \overline{\mathrm{Nu}}_x \,\mathrm{dx}$
t	non-dimensional time, $t = t^* U_0/d$
ν	kinematic molecular viscosity

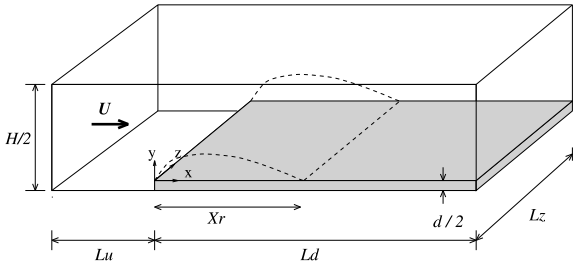

Fig. 1. Topology of the computational domain.

downstream, the free shear layer interacts with the surface of the plate and eventually reattaches. The separation process is often accompanied by what has been termed as "flapping"—a low frequency motion with characteristic frequencies lower than those associated with the Kelvin–Helmholtz and the subsequent shear-layer roll-up (see e.g. Kiya and Sasaki, 1985; Djilali and Gartshore, 1991). In the reattachment region, the flow is characterized by large scale unsteadiness, and pseudo-periodic bursting of the separation bubble and shedding of vorticity. Direct and large-eddy simulations of this flow have underpinned the effect these phenomena have on the dynamics of the flow and on momentum and scalar transport (Tafti and Vanka, 1991; Suksangpanomrung et al., 2000).

The periodically perturbed flow around a flat blunt plate was examined experimentally by Hourigan et al. (1991), who reported a decrease of the mean reattachment length when acoustic forcing is applied at a frequency close to the dominant frequency of the natural vortex shedding. The results also showed a strong coupling between the vortical structures and the thermal field. In the context of this paper, the most relevant work is the experimental investigation of Hwang et al. (1998) who performed detailed measurements of flow over a bluff plate at $Re = 1120$ subjected to a pulsatile free stream. Hwang et al. reported that for low amplitudes forcing, the mean reattachment length drops and then increases in a quadratic manner with increasing forcing frequency. Up to 78% shortening of the mean separation bubble length was reported, and it was noted that the minimum bubble size (or reattachment length) depends more on the forcing frequency than on the forcing amplitude. At higher amplitudes, the variation of the reattachment length was found to oscillate before eventually recovering to the non-perturbed value at higher frequencies. Similar observations were also made by Kiya et al. (1997) for the equivalent axisymmetric geometry (blunt circular cylinder) and for higher Reynolds numbers (order of 10^5).

This paper focuses on two-dimensional simulations which should provide insight into the large scale unsteadiness. The inlet is perturbed sinusoidally over a range of frequencies and amplitudes $A_p \leqslant 0.2$. The effects of the oscillations on the flow dynamics, the temperature field and the wall heat transfer are examined.

2. Methodology

2.1. Governing equations

The Navier–Stokes equations for unsteady, incompressible flow can be written in the following non-dimensional form:

Table 1
Summary of simulation parameters

Grid	$\Delta x_{\min}$	$\Delta y_{\min}$	$H/2$	L_u	L_d	f_p	A_p	$\bar{x}_r$
175×70	1.04×10^{-2}	1.05×10^{-2}	4.5d	10.5d	20d	0, ($3f_n$)	0, (0.05)	6.12, (4.85)
300×100	5.7×10^{-3}	4.13×10^{-3}	4.5d	10.5d	30d	0, ($3f_n$)	0, (0.05)	6.12, (4.15)
450×150	5.7×10^{-4}	5.55×10^{-4}	4.5d	10.5d	30d	0, ($3f_n$)	0, (0.05)	–, (4.27)

$$\frac{\partial U_i}{\partial x_i} = 0 \tag{1}$$

$$\frac{\partial U_i}{\partial t} + \frac{\partial U_i U_j}{\partial x_j} = -\frac{\partial P}{\partial x_i} + \frac{1}{Re}\frac{\partial^2 U_i}{\partial x_j^2} \tag{2}$$

The temperature field is governed by the non-dimensional unsteady energy equation:

$$\frac{\partial T}{\partial t} + \frac{\partial U_j T}{\partial x_j} = \frac{1}{RePr}\frac{\partial^2 T}{\partial x_j^2} \tag{3}$$

where the Prandtl number is given by $Pr = v/\left(k/\rho c_p\right)$.

2.2. Numerical method

The numerical simulations are performed using a staggered grid, finite volume method. All terms, including convective fluxes, are discretized using a second-order central differencing scheme. A low storage third-order Runge–Kutta algorithm is used for time integration in conjunction with a classical correction method at each sub-step. The continuity equation and the pressure gradient term in the momentum equation are treated implicitly, while the convective and diffusive terms are treated explicitly. The linear system for pressure arising from the discretization of the Poisson equation is solved by a direct method.

2.3. Computational domain and boundary conditions

A schematic of the flow domain is shown in Fig. 1. At the inlet boundary, a spatially uniform, time-varying velocity field is specified by $U = 1 + A_p \sin 2\pi f_p t$, where A_p and f_p are the amplitude and frequency of the perturbation.

At the outlet boundary, an advective condition is specified by $\partial U/\partial t + C_u \partial U/\partial x = 0$, where the "advective velocity" C_u is taken as the time-averaged mean (bulk) velocity across the outlet boundary. In strongly advective flows, this approximate treatment of the outlet boundary leads to minimal localized distortion near the outlet. At the top and bottom boundaries, a symmetry condition is used. The no-slip condition is applied along the surface of the plate. The boundary conditions for the energy equation are set as follows: constant free stream temperature at the inlet; convective condition at the outlet ($\partial T/\partial t + C_u \partial T/\partial x = 0$); and constant heat flux along the surface of the blunt plate.

The computations are performed for a plate with a blockage ratio B_r of 10%. The distance from the inlet boundary to the plate is $L_u = 10.5d$. and a downstream boundary is located at $L_d = 30d$. We note that though the configuration and flow regime are close to the case investigated by Hwang et al. (2001), both Reynolds number and blockage ratio differ (1120 and 4.5% in Hwang et al.).

3. Grid sensitivity

A grid sensitivity study was conducted to assess the resolution of the flow in both unperturbed and perturbed regimes. Three different grids were used for this purpose; their features and the parameters for the various simulations are summarized in Table 1. A non-uniform mesh in both x and y directions was used with grids clustered in the vicinity of the leading edge of the plates, where severe gradients are encountered (Fig. 2). The time-step for all simulations were floated and adjusted to satisfy a stability criterion based on the Courant number. Grid sensitivity simulations were performed, in the perturbed cases, for a non-dimensional perturbation frequency of $f_p = 3f_n$, and an amplitude $A_p = 0.05$.

Table 1 shows the variation of the mean reattachment lengths in the unperturbed and perturbed regime, respectively. For the two finer grids, the reattachment lengths are in close agreement in both regimes. Comparison of the mean wall pressure coefficient $\overline{C}_p$ in Fig. 3, shows good agreement of the distributions obtained with all three grids. In the case of the forced regime, a higher resolution is required, and the two finest grids (300×100 and 450×150) provide similar solutions as shown in Fig. 3, with a maximum difference of $< 2\%$. Consequently, the parametric simulations discussed next were all performed using the 300×100 grid (Fig. 4).

4. Results and discussion

4.1. Analysis of the unperturbed flow

Simulations performed over a range of perturbation amplitudes $A_p = 0$–0.2 and frequencies $f_p = f_n$–$10f_n$ ($f_p = f_n$–$60f_n$ for $A_p = 0.2$) are presented and analyzed in this Section.

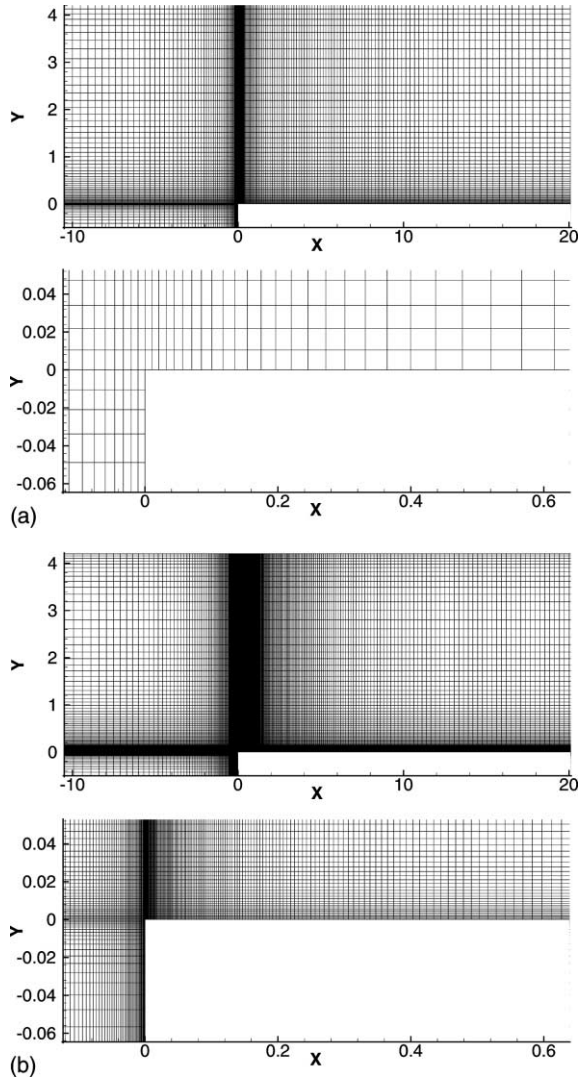

Fig. 2. View and close-up of the (a) 175×70 grid and (b) 450×150 grid (partial view up to $x = 20$).

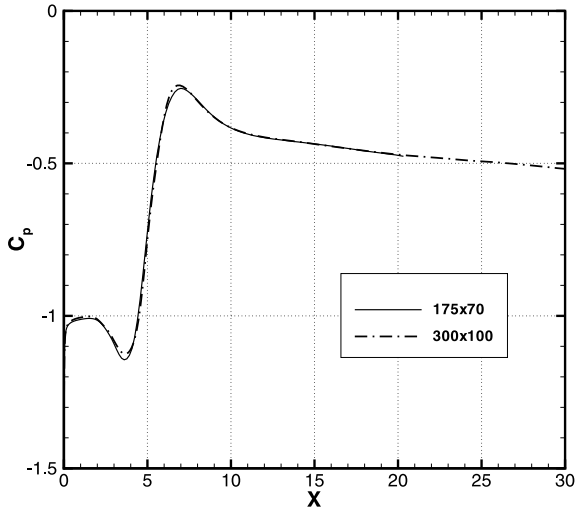

Fig. 3. Effect of grid density on the mean wall pressure coefficient; unperturbed flow.

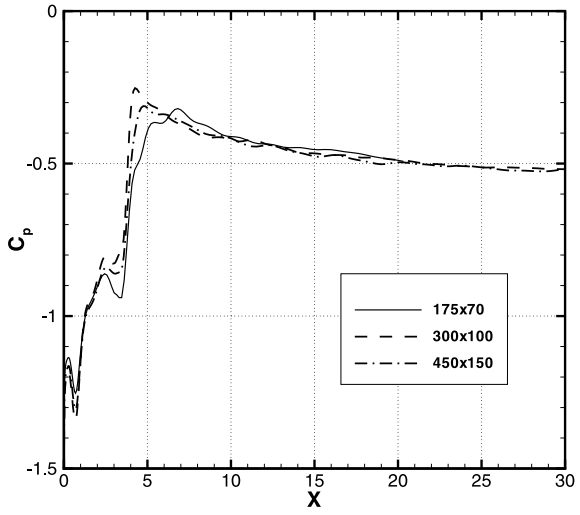

Fig. 4. Effect of grid density on the mean wall pressure coefficient; perturbed flow ($A_p = 0.05$; $f_p = 3f_n$).

The base flow at $Re = 1000$ displays an inherently unsteady behaviour as reported in several experimental and numerical studies (Ota et al., 1981; Tafti and Vanka, 1991). The flow pattern for the unperturbed base case is illustrated in Fig. 5. The instantaneous vorticity field shows the separated shear layer and the typical cycle of vortex formation and shedding. The roll-up process occurs at about $x = 3$, and vortices shed from the previous cycles are located at $x \approx 4$ and 7. At $t = 1510$, while the new vortex is shed and slowly advected, the shear layer starts rolling up forming the core of a new vortex. We note that after $x \approx 6$, which correspond to the time mean reattachment length ($\bar{x}_{rn} = 6.12$), the vortices moving away from the wall are convected at a higher velocity. This typical flow pattern is repeated in a quasi-periodic fashion, with occasional vortex merging taking place. The simulated flow patterns shown reproduce very well the experimental patterns reported by Hwang et al. (2000) using smoke visualization.

The strong correlation of the temperature field with large scale vortical motion is clearly depicted in Fig. 5 (right). The instantaneous wall heat transfer coefficient (not presented here) attains local peaks at locations slightly upstream of each vortex. The local heat transfer enhancement is due to the ejection by the vortex-induced rotational motion of heated fluid away from the surface and entrainment of cooler free stream fluid toward the surface.

By applying a fast fourier transform to the v-component velocity signals along an horizontal line close to the plate surface ($y = 0.5$) and corresponding approxi-

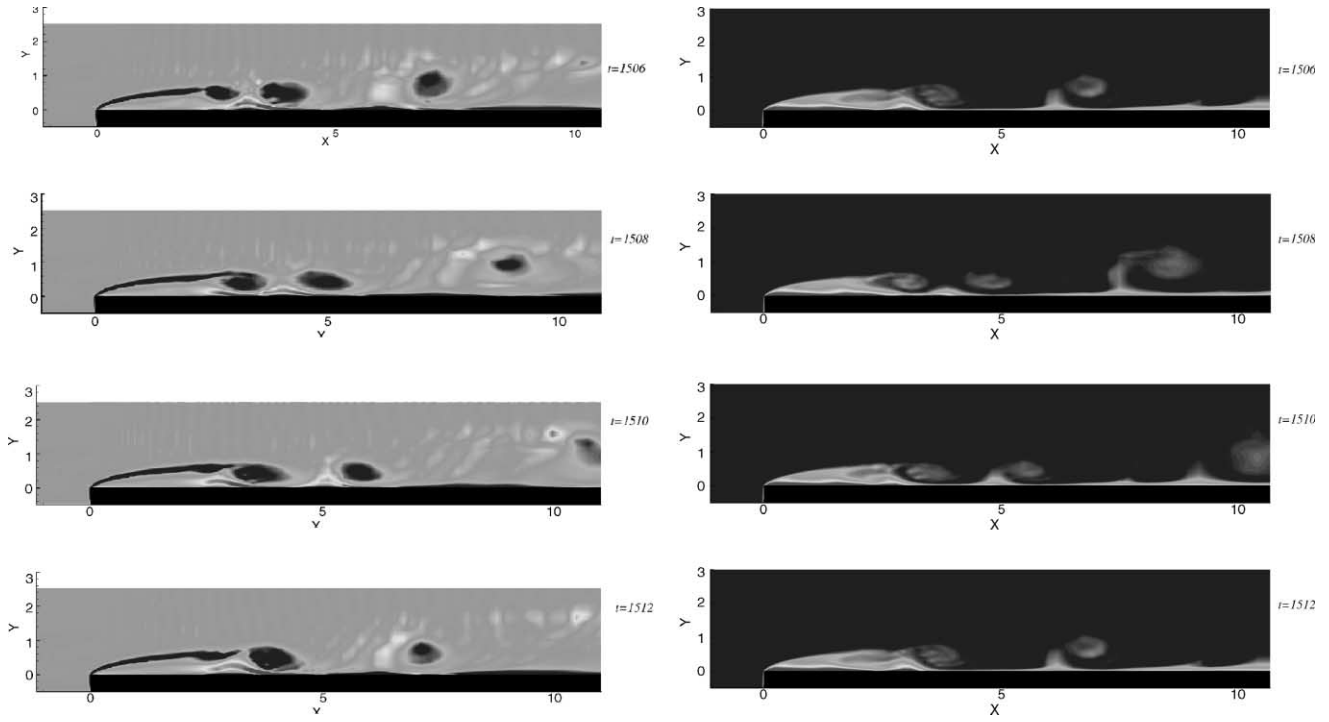

Fig. 5. (Left) instantaneous vorticity field showing a cycle of vortex formation and shedding in the unperturbed flow, $Re = 1000$. (Right) corresponding instantaneous temperature; lighter shades indicate higher temperatures.

mately to the outer edge of the separated shear layer for $x \gtrsim 1$, it is possible to analyze the evolution of the amplitude of the fundamental frequency component of the flow. The dominant frequencies associated with the large scale structures were determined from velocity spectra evaluated at each grid point along the streamwise direction; the resulting variation of the dominant frequency with the streamwise direction is shown in Fig. 6. A high frequency peak appears at ($x \approx 1.45$). Since this frequency correlates with the characteristic size of the vortices bounding the shear layer, the linear drop of the dominant frequency with distance indicates that, between $x \approx 1.5$ and 3.4, the shear layer grows quasi-linearly, like a conventional free shear layer. As the shear layer starts interacting with the wall and vortex shedding begins, at about $x = 3.4$, the characteristic frequency remains constant, $f_n = 0.14$. This is similar to the experimentally observed behaviour of the flow at higher Reynolds number (Djilali and Gartshore, 1991). Closer to the mean reattachment point, shed vortices are convected at a higher and approximately constant speed and the characteristic frequency converges to a value of 0.2. Fig. 6 (bottom) shows the spectral amplitudes corresponding to each location and dominant frequency. The largest energy fluctuations are clearly associated with shedding of vorticity by the separation bubble at the characteristic frequency $f_n = 0.14$. Harmonics of this frequency were selected as forcing frequencies in the simulations with oscillatory inflow.

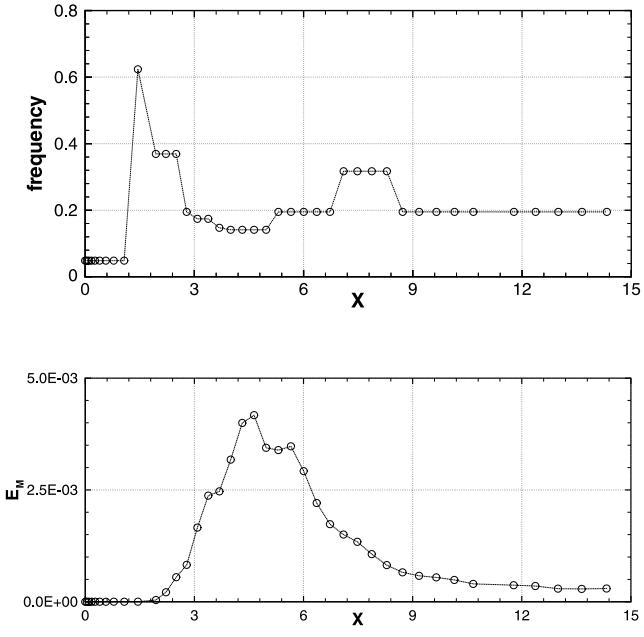

Fig. 6. (Top) variation of the fundamental frequency of the v-component velocity signals along the streamwise direction at $y = 0.5$. (Bottom) corresponding maximum spectral amplitude (E_M) along the streamwise direction; $Re = 1000$.

4.2. Effect of the forcing on the mean and instantaneous flow characteristics

The results for forcing frequencies $0 \leqslant f_p \leqslant 10 f_n$ and a constant amplitude $A_p = 0.05$ are first examined.

A basic characteristic length scale for the flow is the mean reattachment length $\bar{x}_r$, defined as the location of vanishing time-averaged wall shear stress. A value of $\bar{x}_{rn} = 6.12$ is obtained for the unperturbed case, which is in good agreement with the 2D simulations of Tafti and Vanka (1991). The variation of the mean reattachment length (normalized with the unperturbed value $\overline{X}_r = \bar{x}_r/\bar{x}_{rn}$) as a function of frequency is shown in Fig. 7(a) and the corresponding mean streamline patterns are shown in Fig. 7(b). The dynamic response to upstream perturbations radically alters the flow, with forcing at selected harmonics of the fundamental resulting in up to 76% reduction in the separation bubble size. Such radical influence on the mean and dynamic flow characteristics is consistent with experimental observations (Hourigan et al., 1991; Hwang et al., 1998) and will be examined in some details using the present simulations. The computed mean reattachment length in Fig. 7(a), shows a non-monotonic behaviour and a sudden rise at selected frequencies. Detailed examination of the instantaneous vorticity contours in Fig. 8 reveals that this is in fact due to a change of regime of the flow. The flow for both $2f_n$ and $7f_n$ exhibits a typical vortex formation and shedding pattern. In addition, for the case $7f_n$, a merging process takes place around the mean reattachment. A similar phenomenon has also been observed for $3f_n$. As in the unperturbed case, the temperature field in Fig. 9 is again found to be an excellent tracer of the large scale vortical motion.

The "periodic control" of the flow and temperature field by the upstream forcing is clearly illustrated in Fig. 10. The signals taken at locations just upstream of the mean reattachment point show the change from an irregular signal with a clear dominant low frequency activity, in the unperturbed case, to a purely periodic flow in the forced case.

Next we examine the effect of varying forcing amplitudes in the range $A_p = 0.005$–0.2. Forcing frequencies in the range $0 \leqslant f_p \leqslant 10 f_n$ were used; and in one case, $A_p = 0.2$, $0 \leqslant f_p \leqslant 60 f_n$. The variation of the mean reattachment length $\overline{X}_r$ with forcing frequency is shown in Fig. 11(left) for different forcing amplitudes. Each data point on the frequency axis corresponds to the natural frequency and its harmonics. In the case of the smallest amplitude $A_p = 0.005$, $\overline{X}_r$, decreases in a monotonic fashion at the fundamental and the first three harmonic frequencies (f_n–$4f_n$). For the higher frequencies, this parameter oscillates weakly around a value of 0.57.

For $A_p = 0.1$, $\overline{X}_r$ decreases drastically for the first three forcing frequencies. With forcing at the fourth harmonic ($f_p = 0.56$) the value of $\overline{X}_r$ jumps from 0.19 to 1.88, i.e. nearly twice the unperturbed reattachment length. Further increase in the perturbation frequency, results in a drop and then weak oscillations around a value of 0.80.

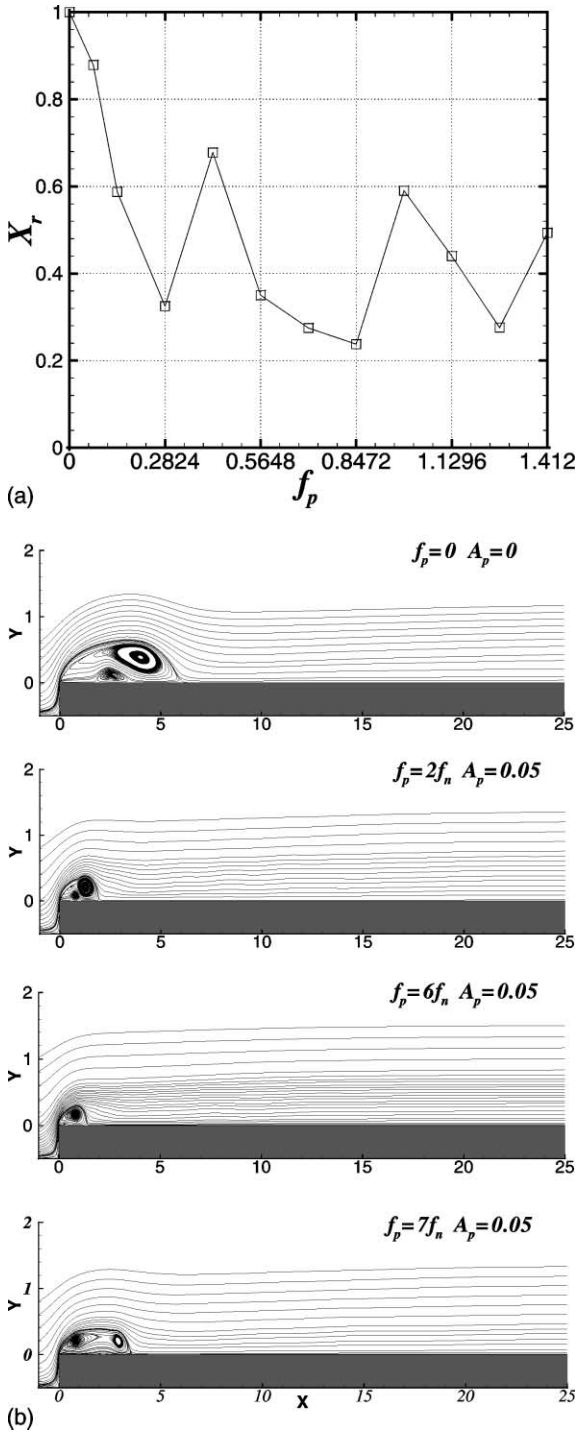

Fig. 7. (a) Variation of the time-averaged reattachement length as a function of forcing frequency. (b) Time-averaged streamline patterns.

The higher amplitude case ($A_p = 0.2$) exhibits a different behaviour. Initially, the reattachment length decreases with increasing f_p and attains the lowest minimum of all simulations with $\overline{X}_r = 0.16$. A rapid recovery follows at higher frequencies with a saturation effect and an apparently asymptotic behaviour with

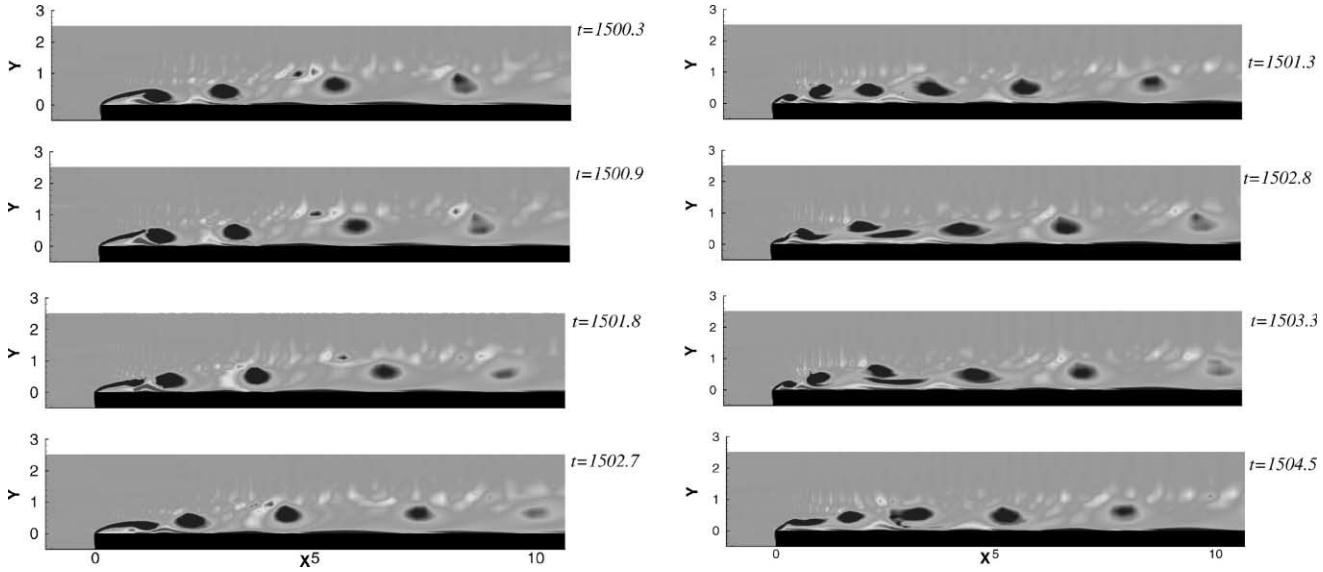

Fig. 8. Vortex pattern sequence during one perturbation period. (Left) $f_p = 2f_n$, (right) $f_p = 7f_n$.

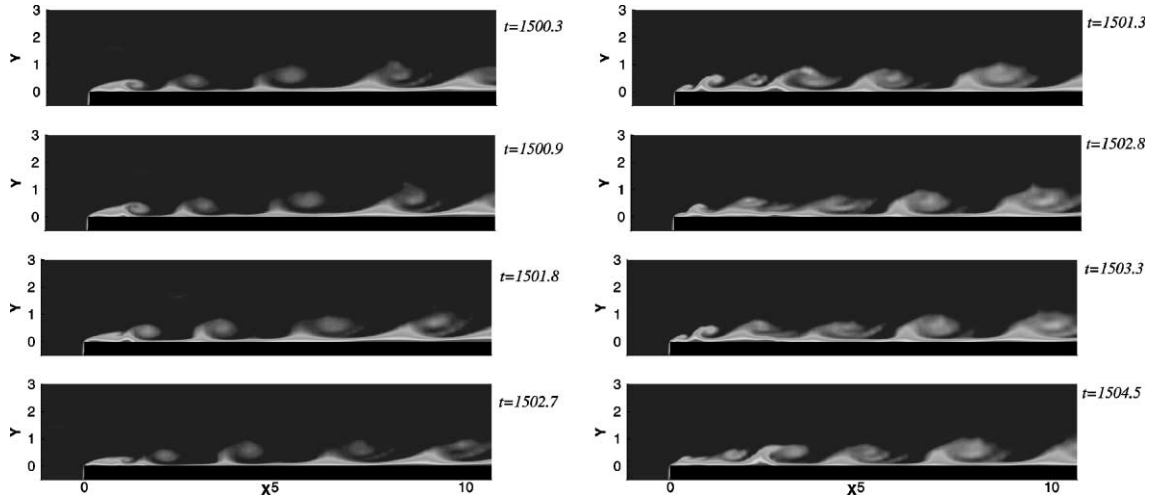

Fig. 9. Temperature field evolution during one perturbation period; lighter shades indicate higher temperatures. (Left) $f_p = 2f_n$, (right) $f_p = 7f_n$.

$\overline{X}_r = 3.15$ at $f_p = 10f_n = 1.4$. Further simulations were performed to explore the response of the flow to even higher frequencies (up to $60f_n$). As shown in Fig. 11(right), a gradual reduction of the reattachment length takes place with increasing perturbation frequency, and by $f_p = 30f_n = 4.2$, $\overline{X}_r$ goes back to its initial non-perturbed value.

The weak oscillations in the value of the reattachment length for low amplitude and low frequency forcing and the return to non-perturbed conditions at higher frequencies are consistent with the experimental observations of Hwang et al. (2001) for the bluff plate and those of Kiya et al. (1997) for the blunt circular cylinder. High frequency, high amplitude cases were not explored by Huang et al. (1998) who used the configuration closest to the present study. Kiya's axi-symmetric configuration and high Reynolds number do not allow for a direct comparison, but we note that a similar return to non-perturbed conditions was observed at high frequencies. In both studies a weak dependence of the minimum reattachment length was noted, and Kiya et al. reported a more complex response of the flow to higher amplitude forcing. The variation of the time-averaged reattachment length at fixed pulsation frequencies as a function of forcing amplitude is shown in Fig. 12. The quasi-asymptotic decrease with increasing forcing amplitude is similar to the experimental results of Hwang et al. (1998) when

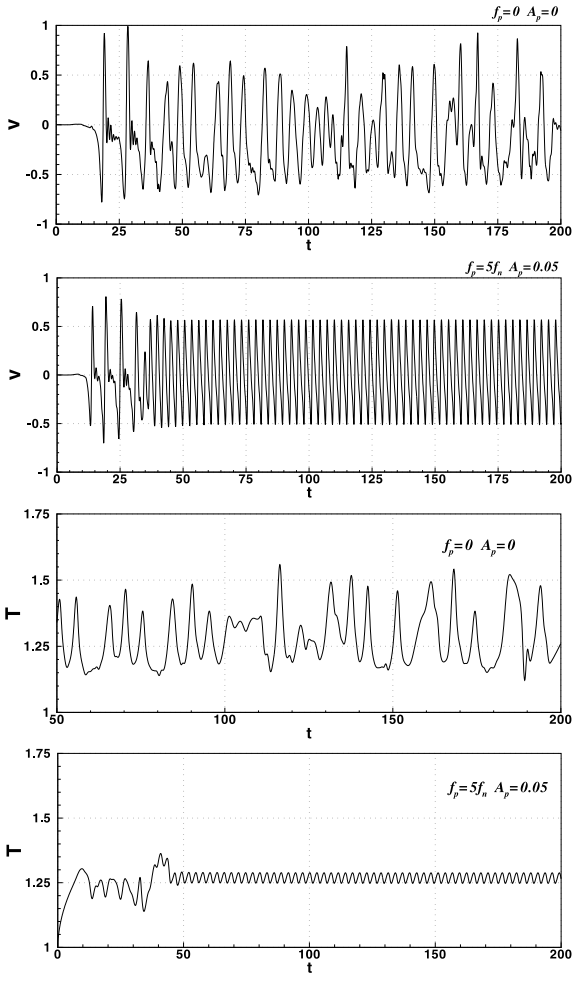

Fig. 10. (Top) velocity traces for unperturbed ($f_p = 0$) and forced flow ($f_p = 5f_n A_p = 0.05$) at $(x, y) = (4.64, 0.5)$. (Bottom) temperature traces at $(x, y) = (4.64, 0.01)$. Time $t = 0$ corresponds to the onset of the upstream perturbation.

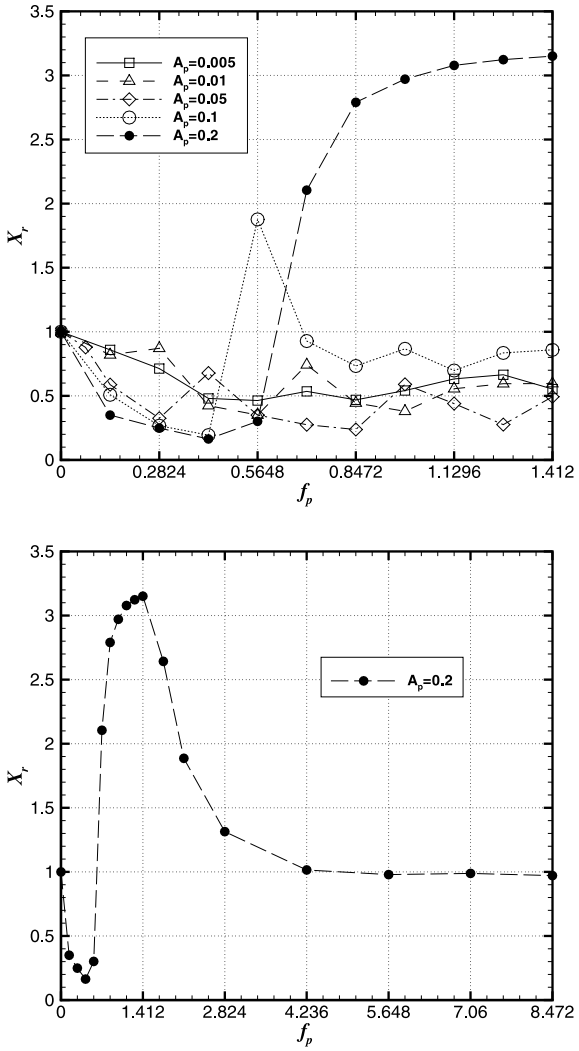

Fig. 11. (Top) variation of the time-averaged reattachement length as a function of forcing frequency and amplitude. (Bottom) effect of forcing with frequencies extended up to $60f_n$ at $A_p = 0.2$.

exciting the flow at low frequencies. Note however that for $f_p = 2f_n$ and $3f_n$, the reduction in $\overline{X}_r$ begins at higher amplitudes.

Representative snapshots of the instantaneous flow for the unperturbed case and for three forced cases with $f_p = f_n$ are shown in Fig. 13. The gradually earlier onset of the vortex roll-up process as the amplitude is increased, is clearly illustrated. This results in earlier interaction of the separated shear layer with the surface of the plate and a shortening of the mean reattachment length that can also be deduced from the figure. The impact of the forcing frequency on the flow dynamics is illustrated in Fig. 14 for $A_p = 0.1$. The vortex shedding occurs at the forcing frequency immediately after separation; the reduced spacing between vortices and the shortening of the separation zone is evident. Close examination of the case $f_p = 4f_n$ shows a regular vortex merging process near $x \simeq 8$, just upstream of the mean reattachment location ($\bar{x}_r = 11.5$). This process is clearly illustrated in the instantaneous flow pattern sequence in Fig. 15. With higher frequency forcing, small size vortices are still generated at the leading edge. However due to the reduced spacing (higher frequency) between successive vortices and the lower advection velocity, as soon as a vortex is shed a second one follows and merges with it shortly after the leading edge of the plate. The resulting vortex (vortex A) has a higher strength (vorticity). The process is followed by further pairing of the two succeeding smaller vortices. The merging process induces a suction effect which leads to a second pairing with vortex A. The second vortex pairing initially tends to reduce the induced velocity on the vortex that follows downstream, as a consequence this vortex is ejected and then advected with the faster outer stream velocity. The location at which the pairing process takes place appear to have a

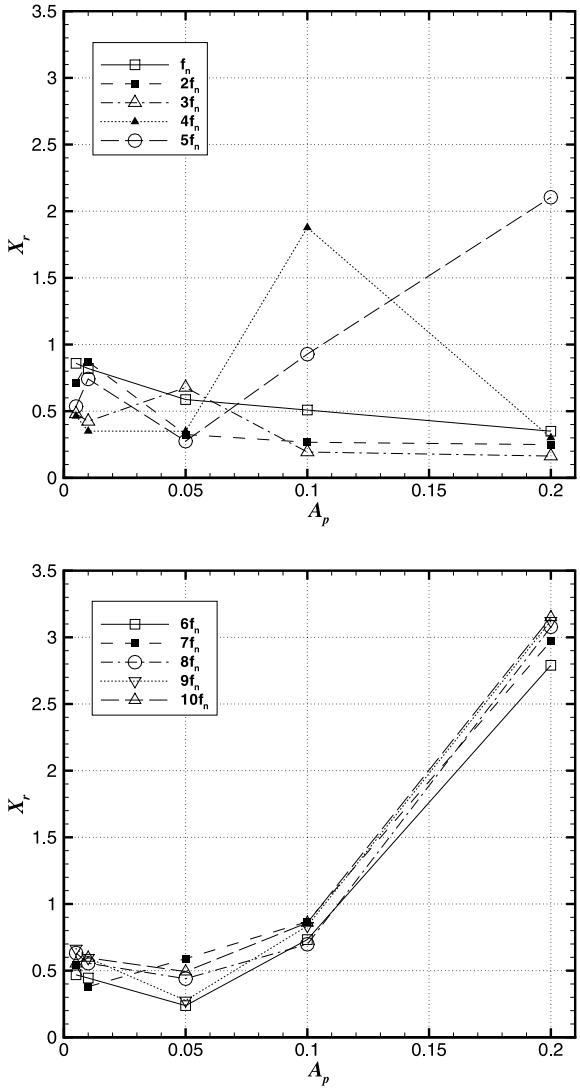

Fig. 12. Variation of the time-averaged reattachement length as a function of forcing amplitude: (top) $f_p = f_n$–$5f_n$, (bottom) $f_p = 6f_n$–$10f_n$.

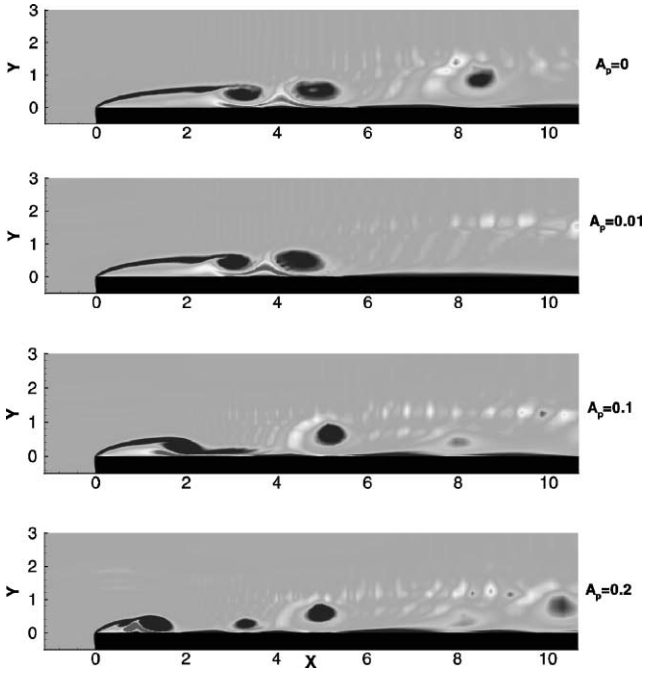

Fig. 13. Effect of forcing amplitude on the vorticity pattern for a fixed pulsation frequency: $f_p = f_n$.

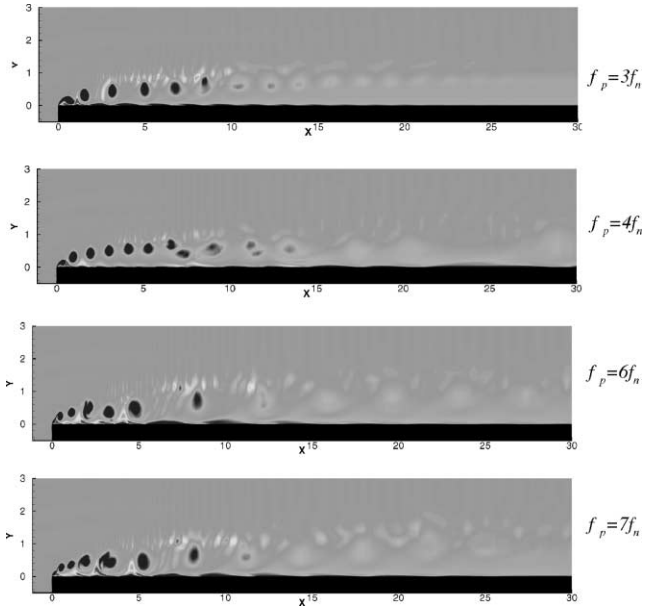

Fig. 14. Instantaneous vorticity pattern at selected frequencies: $A_p = 0.1$.

strong impact on the flow and explain the non-monotonic behaviour of the reattachment length for $A_p \leqslant 0.1$ reported earlier in Fig. 11.

Fig. 16 shows instantaneous flow patterns for the high amplitude case $A_p = 0.2$ at various frequencies. At the lower frequencies, the behaviour is similar to the lower amplitude cases, but no vortex pairing takes place. This is consistent with the monotonic variation of $\overline{X}_r$. As the forcing frequency increases, the vortices in the tail end of the separated shear layer start to diffuse more rapidly and the shear layer stabilizes and becomes quasi-stationary. The onset of this stabilization mechanism occurs further upstream with increasing forcing frequency. By $f_p = 9f_n$, the flow is quasi-steady over most of the plate and the shear layer behaves as a steady laminar shear layer. Its lower growth rate results in delayed interaction with the surface of the plate and, hence, delayed reattachment resulting in a very large separation region. At yet higher frequencies, $f_p > 12.5f_n$, a string of smaller size vortices are still shed from the leading edge. These are convected along the outer edge of the shear layer without penetrating the recirculation zone. This has been experimentally

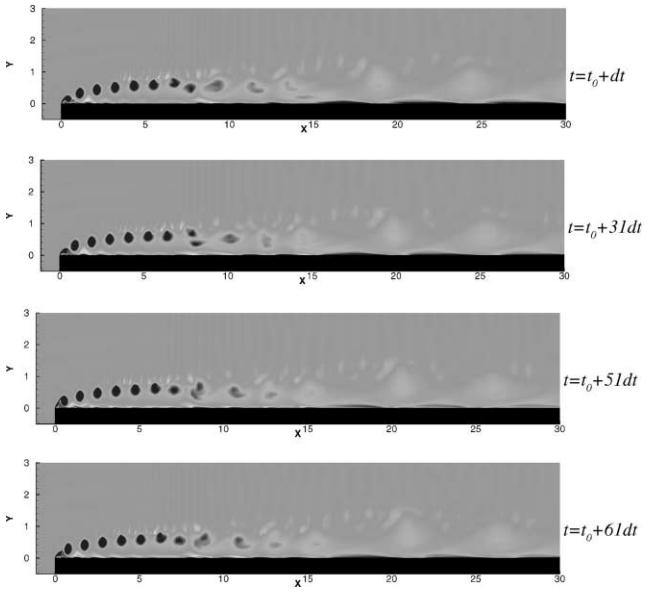

Fig. 15. Flow sequence of forced flow; $A_p = 0.1$ and $f_p = 4f_n$. Vortex merging process occurs near $x \simeq 8$.

observed by Hwang et al. (2001) as well as Chun and Sung (1996). The flow is then governed by two regimes: forcing which controls the flow in the vicinity of the leading edge of the blunt plate, and shear layer instability, as in the unperturbed case, which take place farther downstream.

Fig. 17 shows streamwise velocity signals monitored at three locations: close to the leading edge at $x = 0.5$, $y = 0.2$, approximately midway in the separated shear layer at $x = 2.5$, $y = 0.5$, and at a location corresponding to the unperturbed reattachment zone. Comparing the unperturbed and perturbed case, it is clear that forcing controls the entire flow at low frequencies but has a reduced zone of influence at higher ones. Velocity fluctuation amplitudes of about 0.9 and 0.45 can be observed at $x = 0.5$ and $x = 2.5$ for $f_p = 3f_n$ (Fig. 17b), and with an amplitude of 0.35 for the signal at $x = 5$. With $f_p = 12.5f_n$, the upstream signal is about 0.35 and the downstream signals amplitude is of the same order (0.2). In the recovery regime, $f_p \geqslant 30f_n$, the signal near the reattachment point exhibits virtually the same low frequency characteristics and amplitude as the non-perturbed flow, with the effect of forcing confined to a superposition of a small amplitude high frequency component. Spectral analysis of all recovery regime signals confirm that the two dominant frequencies correspond to the natural vortex shedding frequency (0.14) and the forcing frequency. The signal near the leading edge still exhibits oscillations corresponding to the forcing frequency, but without amplification. In this case, the maximum amplitude approaches the amplitude of forcing (0.2).

4.3. Effect of the forcing on the convective heat transfer

The direct dependence of the temperature field on vorticity was discussed in conjunction with Figs. 5 and 9. Fig. 18 shows the effect of forcing frequency on the distribution of the mean Nusselt number for various amplitudes. With increasing forcing frequency, vortices are shed faster and closer to the leading edge. A larger number of vortices interact with the wall region of the plate, enhancing the vertical motion of warm fluid away from the plate and entraining cooler free stream fluid into the near wall region. This results in significant heat transfer rate enhancement, and an upstream migration of the location of $\overline{Nu}_{x_{max}}$ in tandem with the mean reattachment length. For $A_p = 0.05$, we note that in general the higher heat transfer rates correspond to a lower mean reattachment length, although this is not the case for $3f_n$ and $7f_n$. These cases result in both higher heat transfer rates, and a location of $\overline{Nu}_{x_{max}}$ which is not close to but rather upstream of $\overline{X}_r$. This is attributed to the merging process present at these particular frequencies and which appears to yield further mixing and heat transfer enhancement. In fact, the closer the vortex pairing to the leading edge, the higher is the heat transfer rate ($7f_n$).

Fig. 18b–d and e show the variation for the other forcing amplitudes investigated. The maximum heat transfer increases with increasing amplitude. For $A_p = 0.2$, $\overline{Nu}_x$ exhibits a high value plateau near the leading edge rather than a local maximum. In this case the drop with higher frequencies is faster than for the lower amplitude cases. We also note that all forced cases cross the non-perturbed curve at lower values of $\overline{Nu}_x$ at some distance downstream of separation. The higher the forcing frequency, the shorter the distance at which the perturbed flow becomes less effective than the unperturbed one. The overall heat transfer effectiveness is shown in terms of the average Nusselt number, $I_N = (1/L_d)\int_0^{L_d} \overline{Nu}_x \, dx$, in Fig. 19, and this clearly shows that though the maxima are enhanced with forcing, the overall gain in average heat transfer rates is modest, and in fact a reduction in the mean heat transfer rate occurs for $A_p = 0.2$. Naturally, when the flow returns to the unperturbed solution at high frequencies, the Nusselt number also recovers as shown in Fig. 19b.

5. Conclusions

Two-dimensional simulation of the unsteady separated flow over a bluff rectangular plate subjected to an oscillatory bulk flow were presented and analyzed. The simulations allowed exploration of a broad range of forcing amplitudes and frequencies up to the 60th harmonic of the natural vortex shedding frequency. The

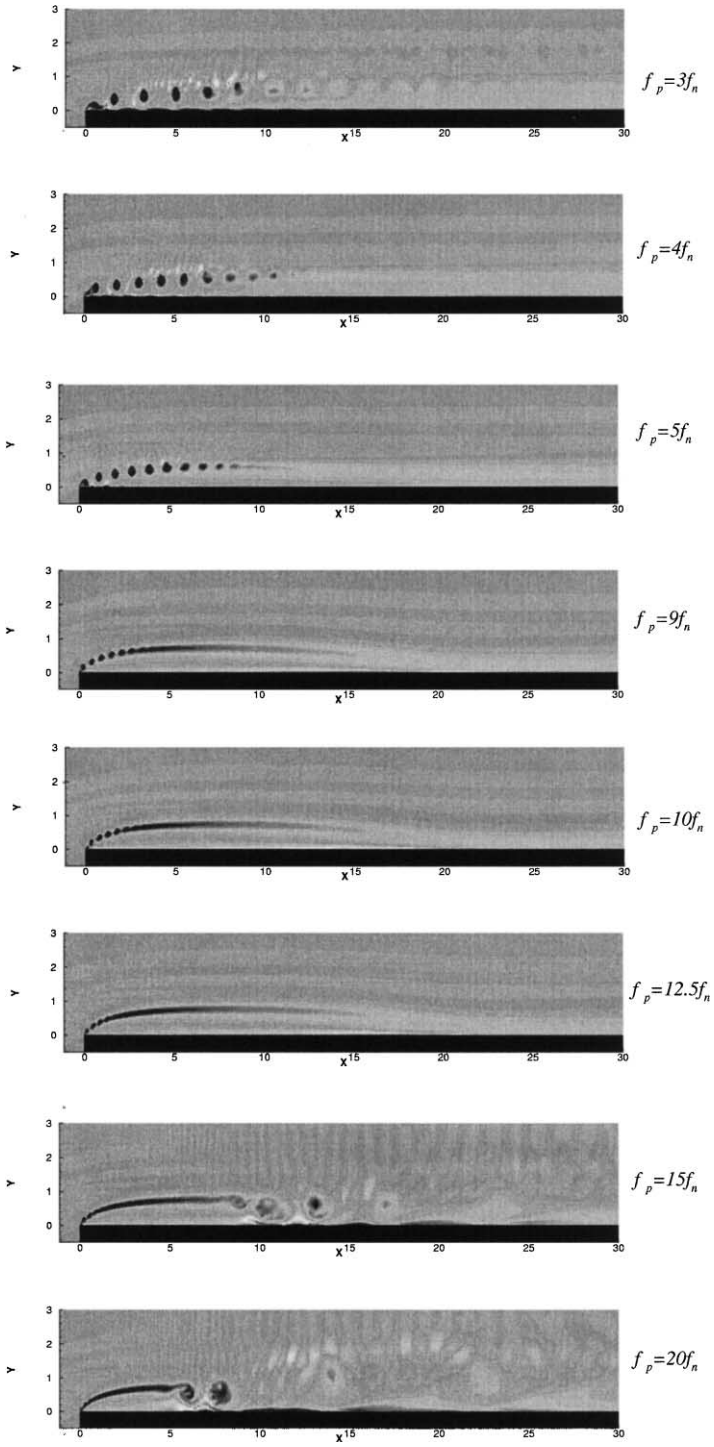

Fig. 16. Vorticity pattern at selected frequencies for $A_p = 0.2$. $f_p = 3, 4, 5, 9, 10, 12.5, 15, 20 f_n$. String of vortices in the separated shear layer is clearly visible as the forcing frequency increases.

results show that forcing has a significant impact on the mean and dynamic characteristics of the flow as well as on the heat transfer. The periodic forcing "controls" the entire flow around the blunt plate. At high forcing frequencies, this control is however confined to a region close to the leading edge of the plate. The highest forcing amplitudes ($A_p = 0.2$) yields the shortest as well as the largest reattachment lengths depending on the forcing frequency. A significant enhancement in the local Nusselt number accompanies the effect of forcing on the

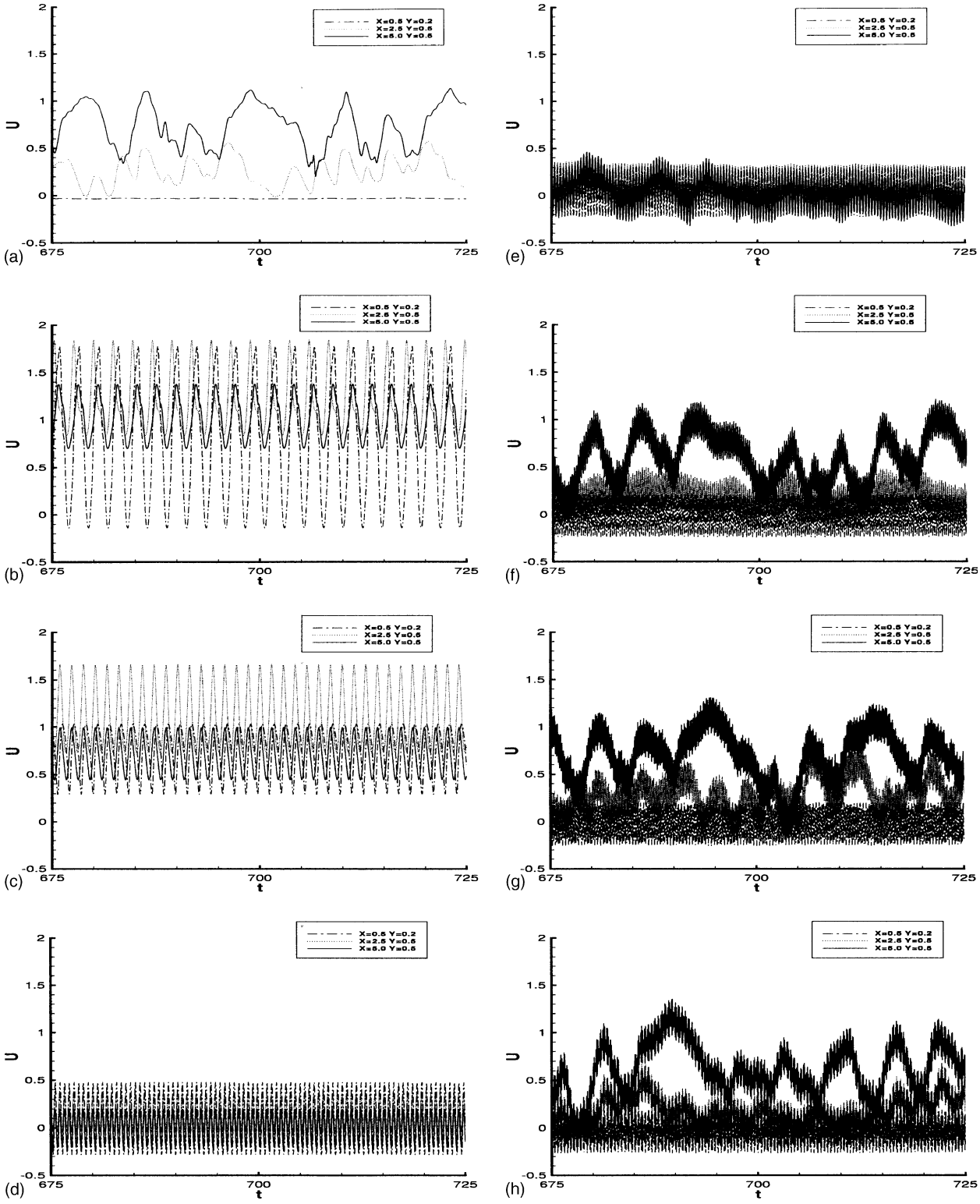

Fig. 17. Traces of U component velocity monitored at ($x = 0.5$, $y = 0.2$), ($x = 2.5$, $y = 0.5$) and ($x = 5.0$, $y = 0.5$): (a) Unperturbed; (b) $f_p = 3f_n$; (c) $f_p = 5f_n$; (d) $f_p = 12.5f_n$; (e) $f_p = 20f_n$; (f) $f_p = 30f_n$; (g) $f_p = 40f_n$; (h) $f_p = 60f_n$. The amplitude of forcing is fixed: $A_p = 0.2$.

flow, however the effect is localized to a small region near the leading edge for high amplitude forcing, and in fact the overall average heat transfer rate is reduced in this case. The present study is a precursor to full three-dimensional simulations that would account for the breakup of spanwise vortices inherent to this type of

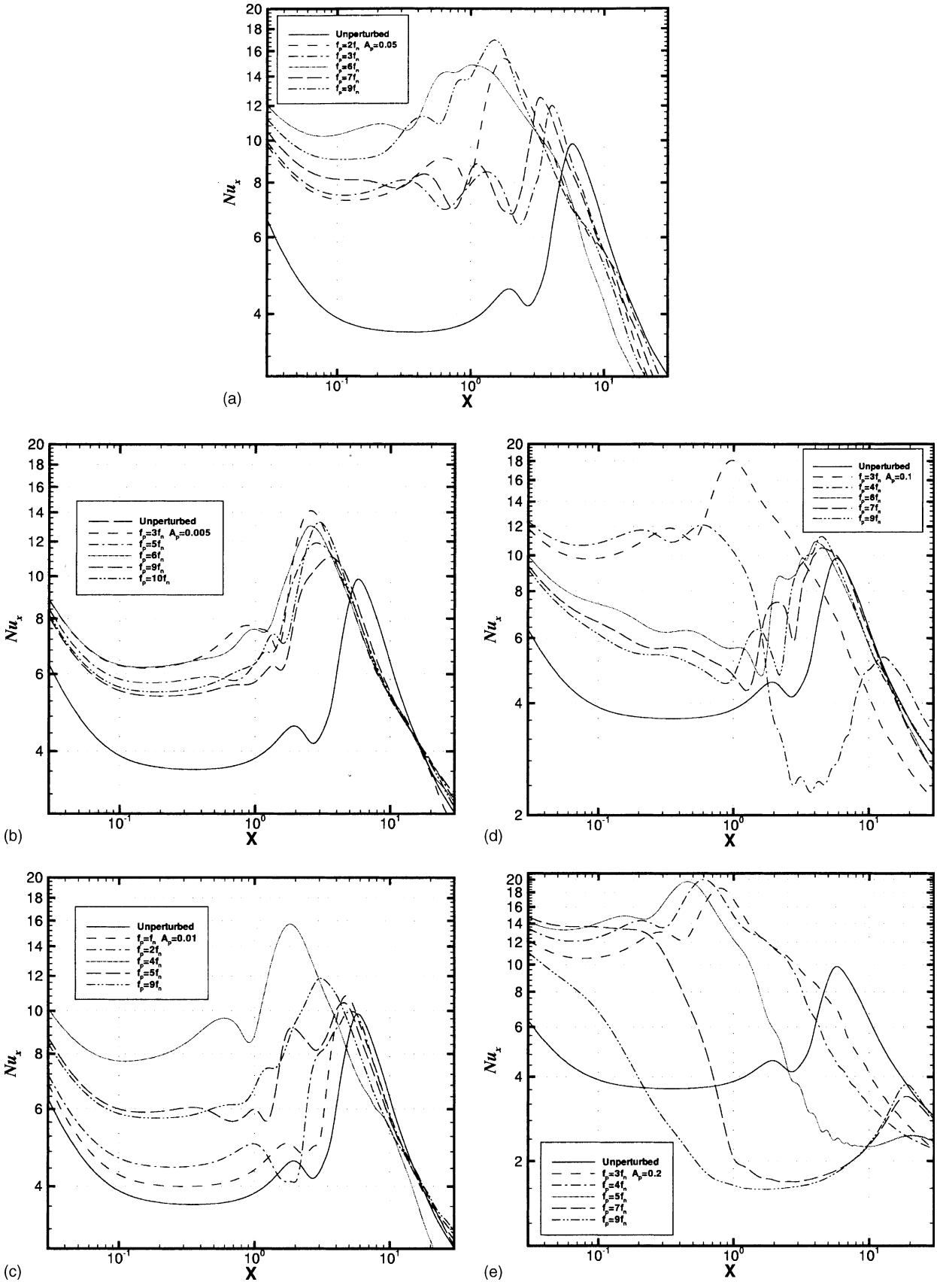

Fig. 18. Variation of the time-averaged local Nusselt number as a function of amplitudes and frequencies: (a) $A_p = 0.05$; (b) $A_p = 0.005$; (c) $A_p = 0.01$; (d) $A_p = 0.1$; (e) $A_p = 0.2$.

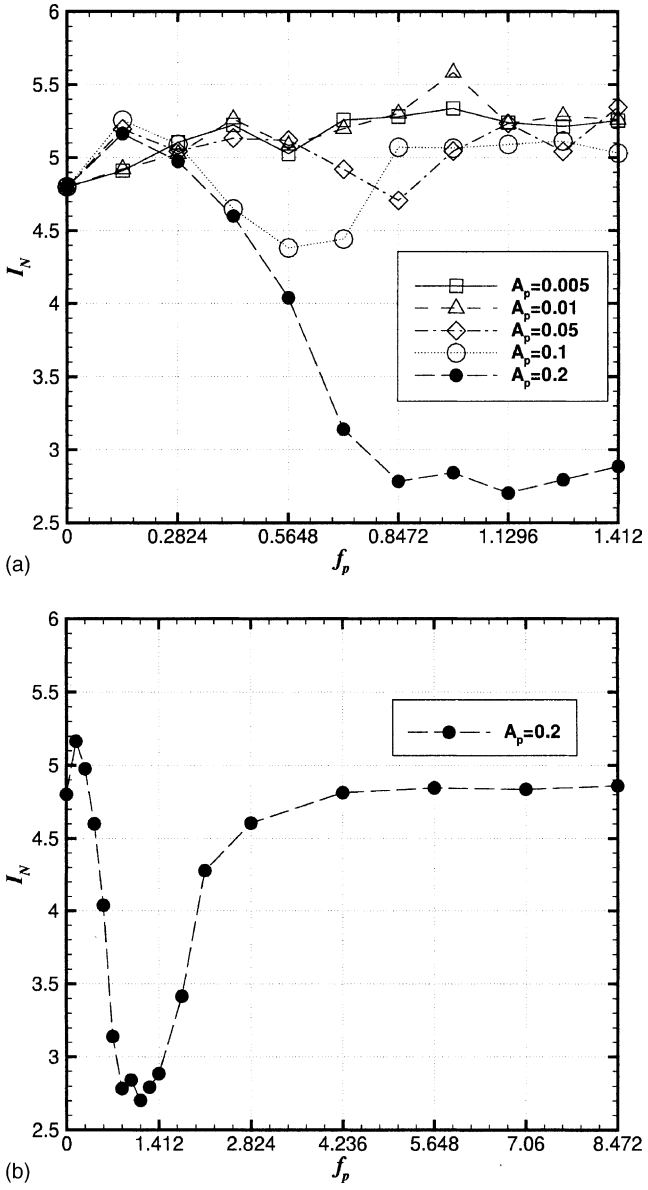

Fig. 19. Average Nusselt number as a function of amplitudes and frequency: (a) lower frequency range; (b) higher frequency range for $A_p = 0.2$.

flow. However the close agreement of the flow patterns with experimental observations, and the low frequency of the forcing and of the natural vortex shedding at the Reynolds number considered indicate that the results should be physically representative.

Acknowledgements

This work was supported by the Natural Sciences and Engineering Research Council of Canada and the University of Victoria.

References

Chun, K.B., Sung, H.J., 1996. Control of turbulent separated flow over a backward-facing step by local forcing. Exp. Fluids 21, 417–426.

Djilali, N., Gartshore, I.S., 1991. Turbulent flow around a bluff rectangular plate. Part I: experimental investigation. J. Fluid Engng. 113, 51–59.

Hourigan, K., Welch, L.W., Thompson, M.C., Cooper, P.I., Welsh, M.C., 1991. Augmented forced convection heat transfer in separated flow a blunt flat plate. Exp. Therm. Fluid Sci. 4, 182–191.

Hwang, K.S., Sung, H.J., Hyun, J.M., 1998. Flow and mass transfer measurements for a flat plate of finite thickness in pulsating flow. Int. J. Heat Mass Transfer 41, 2827–2836.

Hwang, K.S., Sung, H.J., Hyun, J.M., 2000. Visualization of large-scale vortices in flow about a blunt-faced flat plate. Exp. Fluids 29, 198–201.

Hwang, K.S., Sung, H.J., Hyun, J.M., 2001. An experimental study of large-scale vortices over a blunt-faced flat plate in pulsating flow. Exp. Fluids 30, 202–213.

Kiya, M., Sasaki, K., 1985. Structure of large-scale vortices and unsteady reverse flow in the reattachment zone of a turbulent separation bubble. J. Fluid Mech. 154, 463–491.

Kiya, M., Shimizu, M., Mochizuki, O., 1997. Sinusoidal forcing of a turbulent separation bubble. J. Fluid Mech. 342, 119–139.

Orellano, A., Wengle, H., 2000. Numerical simulation (DNS and LES) of manipulated turbulent boundary layer flow over a surface-mounted fence. Eur. J. Mech. B-Fluids, 1–24.

Ota, T., Asano, Y., Okawa, J., 1981. Flow and mass transfer measurements for a flat plate of finite thickness in pulsating flow. Bull. JSME 24, 941–947.

Rosenfeld, M., 1995. A numerical study of pulsating flow behind a constriction. J. Fluid Mech. 301, 203–223.

Tafti, D.K., Vanka, S.P., 1991. A numerical study of flow separation and reattachement on a blunt plate. Phys. Fluids A 3 (7), 1749–1759.

Tutty, O.R., Pedley, T.J., 1993. Oscillatory flow in steped channel. J. Fluid Mech. 247, 179–204.

Suksangpanomrung, A., Djilali, N., Moinat, P., 2000. Large eddy simulation of separated flows over a bluff plate. Int. J. Heat Fluid Flow 21, 655–663.